JACS
JOURNAL OF THE AMERICAN CHEMICAL SOCIETY
Article
pubs.acs.org/JACS

Structural Transition in Myelin Membrane as Initiator of Multiple Sclerosis

Rona Shaharabani,[†,§] Maor Ram-On,[‡] Ram Avinery,[∥,§] Rina Aharoni,[⊥] Ruth Arnon,[⊥] Yeshayahu Talmon,[‡] and Roy Beck*[,∥,§,#]

[†]Raymond & Beverly Sackler School of Chemistry, Tel Aviv University, Tel Aviv 6997801, Israel
[§]Tel Aviv University Center for Nanoscience and Nanotechnology, Tel Aviv University, Tel Aviv 6997801, Israel
[‡]Department of Chemical Engineering and the Russell Berrie Nanotechnology Institute (RBNI), Technion-Israel Institute of Technology, Haifa 3200003, Israel
[∥]Raymond & Beverly Sackler School of Physics & Astronomy, Tel Aviv University, Tel Aviv 6997801, Israel
[⊥]Department of Immunology, The Weizmann Institute of Science, Rehovot 7610001, Israel
[#]Sagol School of Neuroscience, Tel Aviv University, Tel Aviv 6997801, Israel

Supporting Information

ABSTRACT: In demyelinating diseases such as multiple sclerosis, disrupted myelin structures impair the functional role of the sheath as an insulating layer for proper nerve conduction. Though the etiology and recovery pathways remain unclear, in vivo studies show alterations in the lipid and the adhesive protein (myelin basic protein, MBP) composition. We find that in vitro cytoplasmic myelin membranes with modified lipid composition and low MBP concentration, as in demyelinating disease, show structural instabilities and pathological phase transition from a lamellar to inverted hexagonal, which involve enhanced local curvature. Similar curvatures are also found in vivo in diseased myelin sheaths. In addition, MBP dimers form a correlated mesh-like network within the inner membrane space, only in the vicinity of native lipid composition. These findings delineate the distinct functional roles of dominant constituents in cytoplasmic myelin sheaths, and shed new light on mechanisms disrupting lipid−protein complexes in the diseased state.

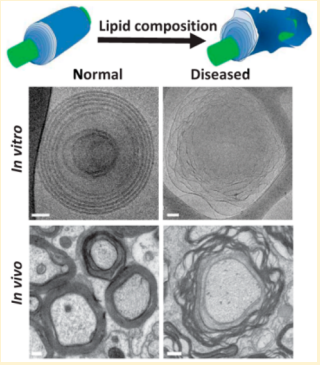

INTRODUCTION

Myelin sheath is a multilamellar complex of lipids and proteins that surround axons,[1] acting as an insulating layer for proper nerve conduction. The sheath nurtures and electrically isolates the axon, speeding up nerve conduction.[2−6] In myelin sheaths, the membrane becomes compact due to electrostatic interactions between the negatively charged lipids and positively charged myelin basic protein (MBP).[7,8] MBP, which represents about 10% of myelin by weight, is intrinsically disordered in solution.[9,10] When bound to a lipid surface, secondary structural elements form, and the hydrophobic parts of the protein are embedded in the bilayer.[11,12] Moreover, the bound MBP has been shown to adopt a compact "C" shape,[13] and to associate with neighboring MBPs to create a mesh-like structure within the cytoplasmic space.[3] Both the topology of the bound MBP structure and the supramolecular organization of the MBP network have been studied extensively with large uncertainties.[12] Importantly, weak transient MBP dimers have been suggested to form the basic building blocks of the network.[12,13] We present new evidence supporting the organization of MBP networks when associated with cytoplasmic myelin membranes.

Multiple sclerosis (MS) is a chronic inflammatory disease of the central nervous system (CNS), correlated with myelin sheath destruction through membrane deadhesion, swelling, and ultimately vesiculation.[4,14−17] Destruction of the myelin sheath in demyelinating diseases, such as MS, results in nerve conduction failure and neurodegeneration (Figure 1A). Experimental autoimmune encephalomyelitis (EAE) serves as an animal model of CNS inflammatory and autoimmunity disorder, in particular MS, because of its many similarities to the disease.[12,18] Loss of adhesion between myelin lamellae and the formation of myelin vesicles have been proposed as possible mechanisms underlying demyelination in MS and EAE.[15]

Previous in vivo studies identified alterations in lipid composition between native (i.e., healthy) and diseased EAE model systems (Table 1, ref 8 and within). The structural consequences of such modifications in composition have not yet been addressed.

Here we investigate the structural implication of lipids and MBP modifications using synchrotron small-angle X-ray scattering (SAXS) and cryogenic transmission electron microscopy (cryo-TEM). We examine the governing interactions between the lipids and MBP. We identify which of these minor lipid-MBP compositions can result in spontaneous

Received: May 17, 2016
Published: August 22, 2016

DOI: 10.1021/jacs.6b04826
J. Am. Chem. Soc. 2016, 138, 12159−12165

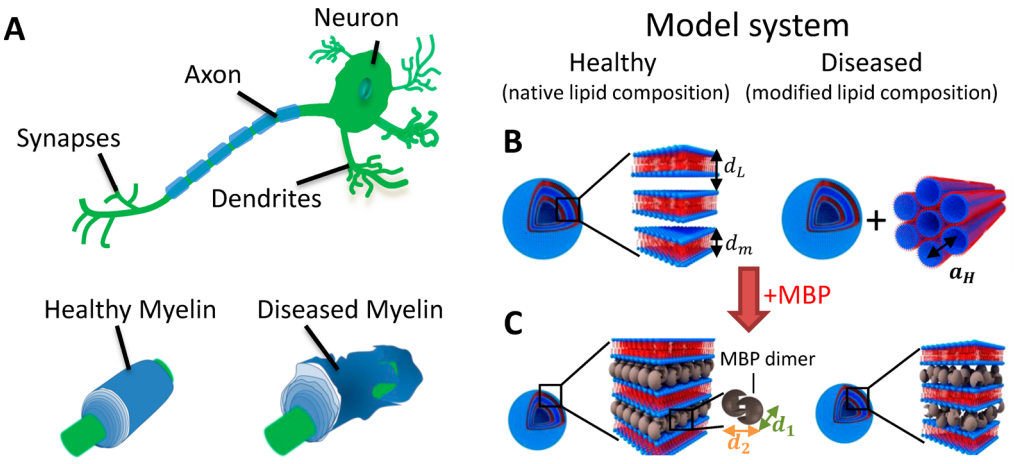

Figure 1. (A) Schematic illustration of a neuron with myelin sheaths wrapped in a spiral around the axon. During neurodegenerative diseases, such as MS, the sheath degrades, exposing the axon. (B,C) MLV model system used to structurally characterize healthy (native, left) and diseased (modified, right) cytoplasmic lipid compositions. (B) In the absence of MBP, the native lipid composition exhibits lamellar packing with membrane thickness d_m and interlamellar spacing d_L. The modified lipid composition shows L_α and H_{II} phases with unit cell length a_H for the latter. (C) MBP inclusion results in a protein dimer network in the native lipid composition and uncorrelated inclusion in the modified lipid composition. The dimers in-plane dimensions are marked by d_1 and d_2.

Table 1. Lipid Compositions of Native (Normal) and Modified (Diseased, EAE) Cytoplasmic Myelin Sheaths (Ref 8 and References Therein)

	mol % lipid	
lipid type	native (normal)	modified (EAE)
Phosphatidylserine (PS^-)	7.0	7.4
Phosphatidylcholine (PC±)	25.9	20.1
Phosphatidylethanolamine (PE±)	29.0	32.9
Sphingomyelin (SM±)	6.2	2.2
Cholesterol (CHOL)	31.6	37.4

structural phase transition. This may suggest new avenues for MS treatment and diagnostics, focusing on specific lipid synthesis and metabolism.

RESULTS AND DISCUSSION

SAXS was used to examine the structure of multilamellar vesicles (MLVs) with native myelin lipid composition, and the structural changes in modified lipid composition that mimic those of cytoplasmic myelin membranes in EAE (Figures 1B,C). Figure 2A shows the high-resolution synchrotron SAXS patterns of native (red) and modified (black) lipid compositions of cytoplasmic myelin. The scattering profiles are composed of prominent Bragg reflections overlaid on the membrane form-factor signal. From the Bragg reflections we calculate the membrane unit cell length and mesophase structure. Multilamellar and hexagonal phases reflections result in $q_{L(00n)} = \frac{2\pi n}{d_L}$ and $q_{H(hk)} = \frac{4\pi}{\sqrt{3}\,a_H}\sqrt{h^2 + hk + k^2}$, respectively. Here q is the scattering wave-vector, and n, h, and k are integers; d_L and a_H represent the real-space unit cell length in each respective phase.

Bragg reflections of native composition (red arrows, Figure 2A) at wave-vectors: $q_{L(001)} = 0.0555$ Å^{-1} and $q_{L(002)} = 0.113$ Å^{-1} fit the L_α multilamellar phase, with an interlamellar spacing of $d_L = 113$ Å. The interlamellar spacing encompasses the thickness of a membrane bilayer (d_m) with a water layer between the head groups (d_w).

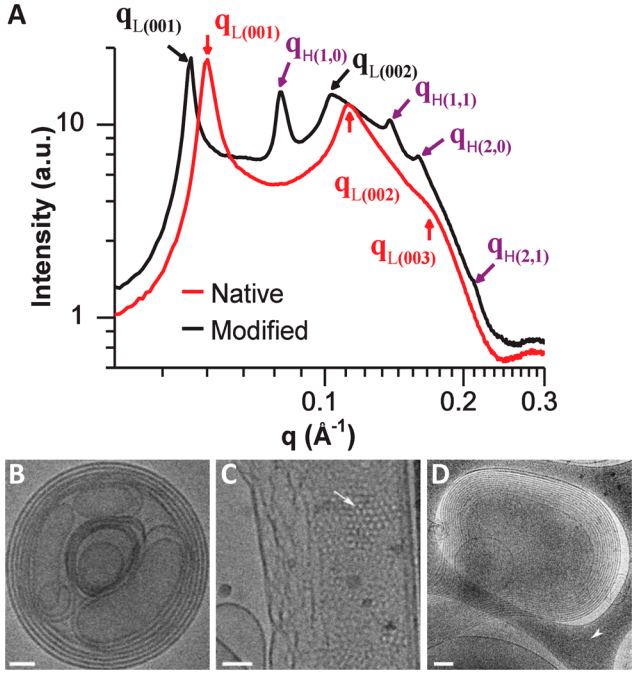

Figure 2. (A) SAXS intensity profiles of MLV with native (red) and modified (black) lipid compositions. In the modified lipid composition, the characteristic correlation peaks are indexed to H_{II} (purple arrows) coexisting with L_α (black arrows). In the native lipid composition, L_α is indexed (red arrows). (B) Cryo-TEM images of MLV, showing native lipid composition and (C,D) modified lipid composition. Hexagonal phase formation is indicated by the arrow in (C), coexisting with the lamellar phase (D); perforated carbon film is indicated by the white arrowhead. Scale bars = 50 nm (B,C) and 100 nm (D).

The bilayer thickness can be directly evaluated by fitting the form-factor scattering profiles to the data with a multilamellar stack of infinite flat membranes, with three-box model electron density profiles for the headgroups, hydrocarbon tails and water layers (Figure SI-1).[19] This analysis gives membrane thickness $d_m = 50$ Å, yielding a water layer thickness of $d_w = 63$ Å. The

DOI: 10.1021/jacs.6b04826
J. Am. Chem. Soc. 2016, 138, 12159−12165

MLVs are kept fully hydrated with excess buffer, suggesting balanced intermolecular forces at this equilibrium spacing with a considerable amount of water within the bilayers.

Unlike the scattering profile of the native composition, the profile of the modified composition has additional distinct Bragg reflections. For modified lipid composition, the reflections at $q_{L(001)}$ = 0.051 Å^{-1} and $q_{L(002)}$ = 0.103 Å^{-1} result from an L_α phase with a repeating distance of d_L = 123 Å (Figure 2A, black arrows). The remaining reflections at $q_{H(1,0)}$ = 0.080 Å^{-1}, $q_{L(1,1)}$= 0.138 Å^{-1}, $q_{H(2,0)}$ = 0.160 Å^{-1} and $q_{H(2,1)}$= 0.210 Å^{-1} result from an H_{II} phase, with a lattice parameter of a_H = 90 Å (Figure 2A, purple arrows). It should be noted that the lamellar $q_{L(002)}$ reflection appears to be convoluted with another weak correlation reflection. The q value resembles that of a cholesterol correlation peak that had been previously characterized.[20]

To validate our scattering data, we imaged the two lipid compositions using cryo-TEM (see Supporting Information). The native composition indeed shows a multilamellar structure typical of an L_α phase (Figure 2B). Notably, the modified lipid composition sample consists of L_α and H_{II} phases, coexisting within the same field of view (Figures 2C, D). These results are in agreement with the scattering data presented above. The native composition shows a multilamellar structure typical of an L_α phase, with an interlamellar separation of 113 Å, and a bilayer thickness of 50 Å (Figures 3A, B). In modified lipid composition samples, MLV with a lamellar separation of ∼120 Å (Figure 3C), and an H_{II} phase with a lattice parameter of ∼90 Å, was recorded, in agreement with the SAXS data. The coexisting H_{II} phase is more pronounced in thicker lipid layers, in which rippled lamellar structures decorate its periphery (Figure 2C), following condensation with centrifugation. Such behavior is typical for hexagonal phases, and had been previously documented.[21]

To further examine the role of each of the lipid modifications, and determine which induces the H_{II} phase formation, we gradually changed each lipid mole fraction, while keeping the remaining lipids at a constant relative mole fraction, as in the original lipid composition. We find that modifying a single component does not induce H_{II} phase formation. Nevertheless, when altering the modified lipid composition with a single component, we find that even minor mole fraction alterations can abolish the H_{II} phase (see Supporting Information and Figures SI-2, SI-3). These results suggest that specific lipid composition tightly regulate the H_{II} phase presence. Therefore, other minor lipid composition inclusions, such as phosphoinositides or phosphatisylinositol,[22] may also regulate the H_{II} phase existence.

The L_α to H_{II} phase transition has been studied intensively.[21,23] The lipid packing shape is a critical factor in setting the spontaneous curvature of the membrane and the resulting mesophase.[24] For the L_α phase, the packing parameter is near unity, with zero spontaneous curvature, whereas the H_{II} phase is induced by a larger packing parameter and negative spontaneous curvature.

Examining the modified lipid composition, we found that the dominant changes tended to increase the overall packing parameter and negative spontaneous curvature (Table 1). The lipid packing parameter is determined by the ratio of the effective lipid chains volume to the headgroup area at the aggregate surface, and the hydrocarbon chain fully extended length.[24] Double-chain lipids with small headgroups areas, such as phosphatidylethanolamine (PE), form inverted structures,

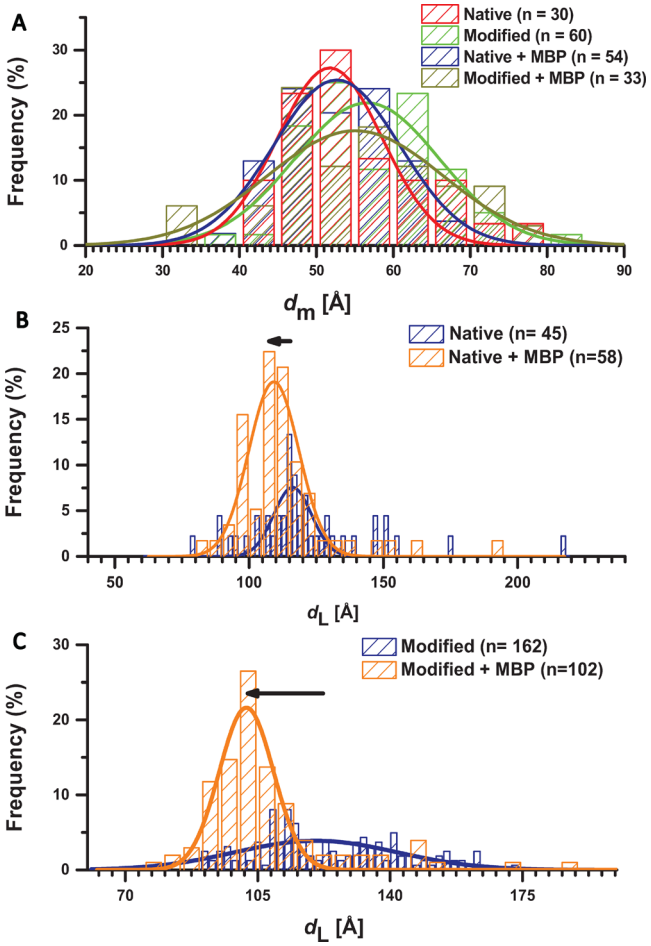

Figure 3. TEM structural analysis for native and modified lipid compositions. (A) Membrane thickness (d_m) as measured for both native and modified lipid compositions, with and without 20 wt % MBP. In all cases the bilayer thickness was found to be, on average, about 50 Å. Intermembrane distance (d_L) frequency with and without 20 wt % MBP for (B) native and (C) modified lipid composition. In both cases, the unit cell spacing is reduced when MBP is added to the mix (black arrows). In native and modified lipid composition samples, MLV with a lamellar separation of 109 and 120 Å were noted, in agreement with the scattering data. Numbers of relevant analyzed cross sections, *n*, are indicated in the legends.

including an inverted hexagonal phase (H_{II}). Anionic lipids with divalent salts, such as phosphatidylserine (PS) with calcium, or double chain lipids with large headgroup areas (e.g., phosphatidylcholine, PC) form flexible membranes.[24] Therefore, mixed lipid membranes can result in local structural instabilities and mesophase coexistence. These local instabilities, which in turn may induce packing stress, which in turn, affect membrane integrity, and influence the insertion, conformation, or activity of membrane-embedded proteins.[25]

Comparing the modified lipid composition to the native one (Table 1), we indeed find that the dominant alterations correspond to an increase in the overall packing parameter, with a tendency to negative spontaneous curvature. This includes an increase of PE content, which has negative spontaneous curvature,[25] and decrease in PC and sphingomyelin (SM) contents, both having slightly positive spontaneous curvature.

We emphasize that only multiple repeating units will yield SAXS correlation peaks. Therefore, local and small "rafts" or

DOI: 10.1021/jacs.6b04826
J. Am. Chem. Soc. 2016, 138, 12159−12165

irregularities in the lamellar spacing cannot explain our data. We suggest that the L_α–H_{II} coexisting phases arise from large-scale membrane rearrangements, in agreement with lower spontaneous curvatures in the modified lipid composition.

Moreover, for lipid complexes, as in our case, macroscopic spontaneous curvature realization might not adequately describe the system, and local phase segregation can occur as well.[26] In addition, modified lipid composition can be related to fluidity and lipid domain distributions. These, in turn, can affect MBP adhesion to the different leaflet stoichiometries.[26−28] Modifications in lipid stoichiometry can therefore increase myelin fluidity, decrease myelin adhesion, increase membrane curvature, and promote vesiculation in the disease state.[15]

Enhanced spontaneous curvature toward the H_{II} phase is also manifested by increased membrane roughness. Such increased membrane roughness is seen both in vitro and in vivo (Figure 4 and Figure SI-4). For perfect spherical shape of radius R, local curvature statistics have a singular population of 1/R value.

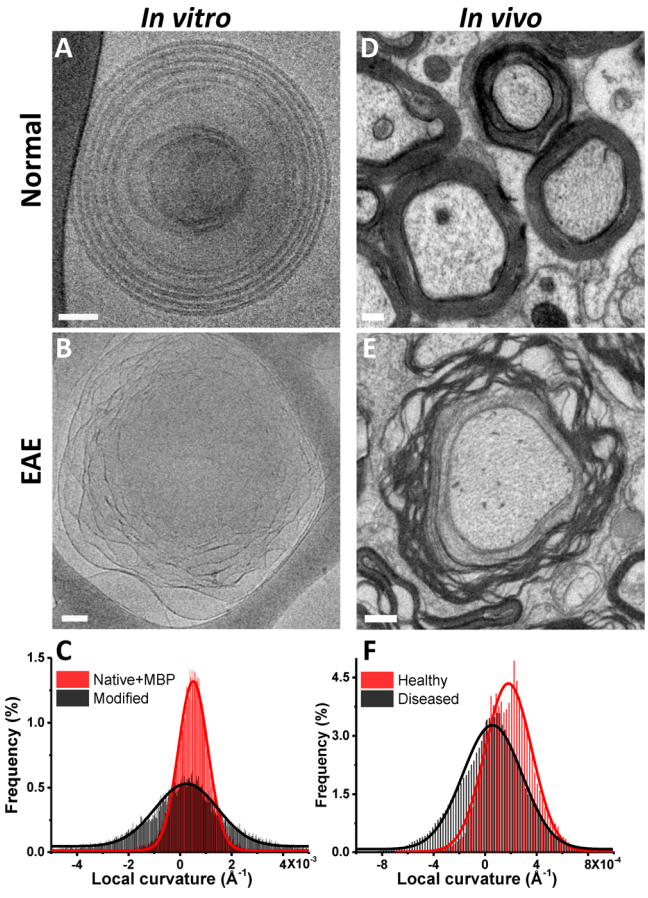

Figure 4. (A) Cryo-TEM images of in vitro native lipid compositions with 20 wt % MBP MLV, and (B) modified lipid composition. Enhanced membrane roughness is shown in the modified lipid composition as depicted from the larger STD of the local curvature frequency analysis (C). Native and modified lipid compositions result with mean local curvature of 4.96×10^{-4} Å^{-1}, 2.14×10^{-4} Å^{-1} and STD of 7.71×10^{-4} Å^{-1}, 2.30×10^{-3} Å^{-1} respectively. TEM images of in vivo transverse cervical sections from (D) normal, and (E) EAE-induced mice. (F) In vivo myelin local curvature show mean local curvature of 1.91×10^{-4} Å^{-1}, 4.410×10^{-5} Å^{-1}, and STD of 1.93×10^{-4} Å^{-1}, 2.69×10^{-4} Å^{-1}, as measured for normal and EAE myelin, respectively. Scale bars = 50 nm (A), 200 nm (B and D), and 500 nm (E).

Hence, for MLV, we expect to have rather sharp distribution around the mean curvature. For membranes with large undulations, as in the vicinity of the H_{II} phase, local curvatures result in significant deviations from the mean local curvature value. This causes larger standard deviation (STD) of the local curvature population.

The in vitro models for native lipid composition result in spherical MLV (Figures 4A and Figure SI-4B). On the contrary, large membrane roughness is found in modified lipid composition model system (Figure 4B and Figure SI-4A). There, the membrane's floppiness is evident visually from the membrane undulations compared to a spherically shaped membrane. in vivo spinal cords dissections of myelinated axons exhibit similar features. There, EAE induced specimens (Figure 4E) show increased myelin roughness in comparison to normal mice (Figure 4D).

We evaluated the membrane roughness of the in vitro MLV model systems, and compared it to measurements of in vivo pathology specimens of EAE-induced mice, as well as normal controls (see Supporting Information). Indeed, we find that both in vivo and in vitro systems have increased probabilities of large local curvatures in the diseased state in comparison to the normal state (Figures 4C, F, Figure SI-4C).

The addition of MBP to the lipid complex has a dramatic effect on the structures of both lipid compositions. The scattering profiles arising from different concentrations of MBP have two distinguishing features. First, the addition of MBP compacts the membrane up to 88 and 84 Å for native and modified lipid compositions, respectively (Figure 5). With increasing MBP concentrations the dominant lamellar peaks (Figure 5, purple and black arrows) shift to higher wave-vector values for both native and modified lipid compositions. This leaves an intermembrane layer thickness of ∼30−40 Å for both compositions. This layer thickness is about half of the aforementioned thickness without MBP inclusion.

Second, the inclusion of MBP caused different structural changes in the two lipid compositions. The one lamellar phase peak, in the native composition, shown in the absence of MBP quickly transitions into three correlation peaks with associated harmonics (blue, green and purple arrows in Figure 5A). Each of the three correlation peaks displays an additional harmonic at double the wave-vector (Figure 5C). These multiple correlation peaks indicate three unit cell distances. Two of the peaks (with the largest correlations lengths) do not shift when the MBP concentration is altered (d_1 = 108 Å, d_2 = 95 Å) while the third dominant lamellar phase, and its associated correlation peaks (Figure 5A, purple arrows), spacing compacts with the addition of MBP from 93 to 88 Å (Figures 5A, C). The dominant peak corresponds to the lipid bilayer distance (L_α phase), whereas the two shallow peaks correspond to lateral MBP correlations (Figure 1C). Although the second harmonics of the shallow peaks are clearly observed (Figure 5C), the absence of the (1,1) correlation indicates the lack of long-range 2D lattice, as previously suggested.[12]

With the modified lipid composition, the coexisting L_α–H_{II} phases quickly lead to a single, sharp lamellar phase (Figure 5B, C). The lamellar phase is compressed as MBP concentration increases (1−20 wt %), from 94 to 84 Å. In contrast to the native composition, the lamellar correlation peaks in the modified lipid composition with MBP (Figure 5B) are significantly more prominent, and display up to four harmonics. There, the MBPs are unable to form mesh-like structures

DOI: 10.1021/jacs.6b04826
J. Am. Chem. Soc. 2016, 138, 12159−12165

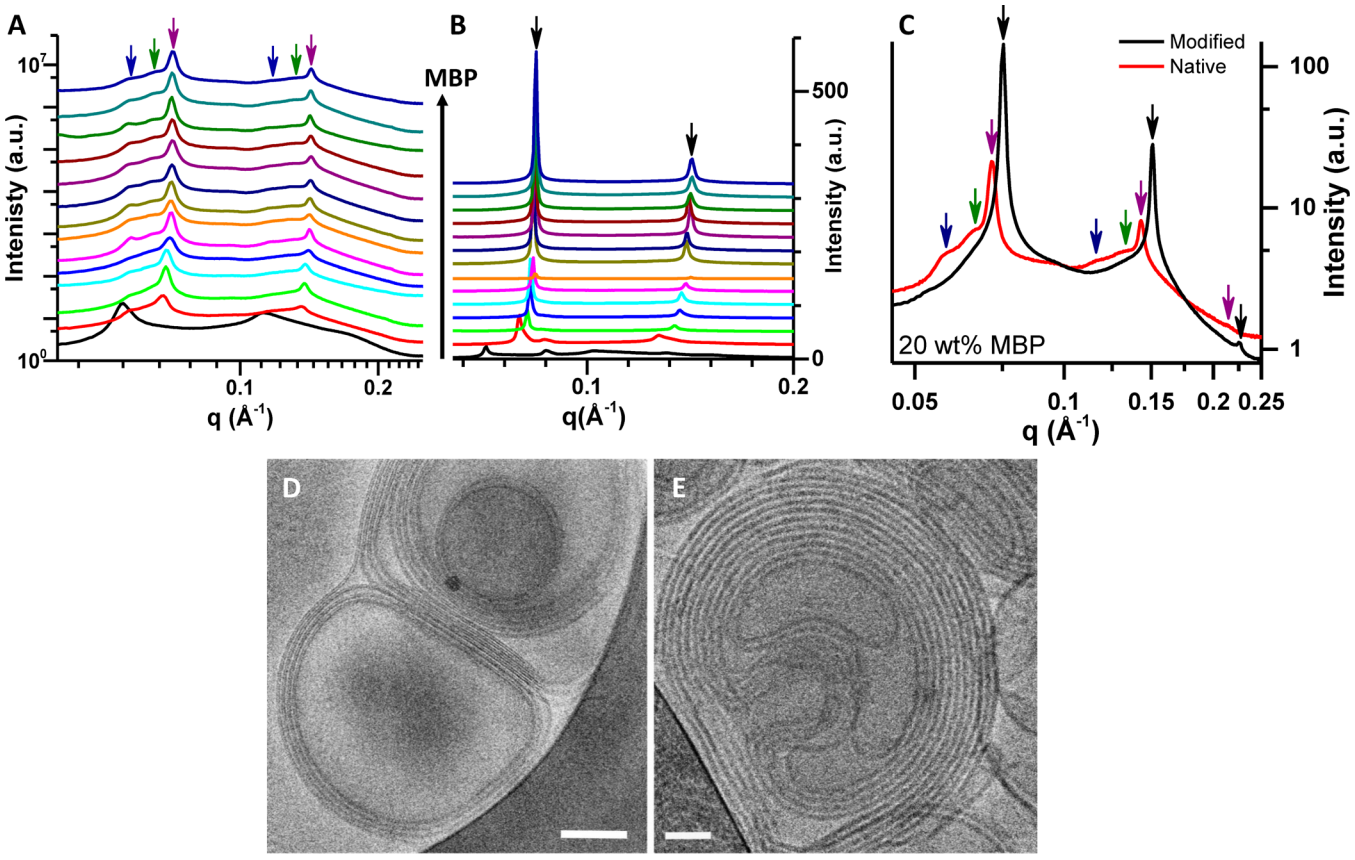

Figure 5. SAXS profiles of (A) native and (B) modified lipid composition with increasing MBP concentrations (bottom to top, 0−10 wt % at 1 wt % increments, 13, 15, and 20 wt %). While dominant lamellar phases (purple and black arrows) shift up to intermediate MBP concentration, subdominant correlation peaks (blue and green arrows) appear only for native composition, and remain stationary. For clarity of presentation, the profiles are vertically shifted. (C) SAXS profiles of native (red curve) and modified (black curve) lipid composition with 20 wt % MBP. The dominant peaks, and their three associated harmonics, are marked with purple and black arrows for native and modified lipid compositions, respectively. Those peaks correspond inversely to the interlamellar spacing. The two shallow correlation peaks, with noticeable second harmonics, are present only in the native lipid composition (blue and green arrows). These shallow peaks represent the MBP dimer network unit cell. Cryo-TEM images of (D) native and (E) modified lipid compositions with 20 wt % MBP MLV. Scale bars = 100 nm (D) and 50 nm (E).

(Figure 1C), but effectively change the spontaneous curvature of the membrane.[29]

The structural organization of both native and modified lipid composition in the presence of MBP uptake was further investigated using cryo-TEM (Figures 5D, E). Both lipid compositions show a membrane thickness of about 50 Å (Figure 3A) and lamellar structures in which the hexagonal phase was absent (Figures 5D, E). Moreover, the interlamellar spacing, as imaged by cryo-TEM and by SAXS, becomes more compact with the inclusion of MBP (Figures 3B, C and Figures 5D, E). Statistical characterization of the cryo-TEM images clearly indicates a much wider distribution of interlamellar spacing in the absence of MBP (Figure 3B, C), in agreement with the structural instabilities seen in such complexes, and only a lamellar phase when MBP is included.

Apart from small deviations from the modified lipid composition, the incorporation of MBP yields SAXS profiles with the three aforementioned correlation lengths. This finding indicates that the presence of MBP is crucial for stabilizing the complex, regardless of its lipid composition. Moreover, MBP causes the leaflets to adhere to one another, and flattens the membranes, counteracting local negative curvatures. Recently, Aggarwal et al. demonstrated a process by which MBPs interact via hydrophobic phenylalanine residues.[3] These cooperative interactions result in protein networks and macroscopic phase separation, inducing membrane zippering within the cytoplasmic leaflet.[3,5,13]

When bound to membranes, the MBP dimensions[30] are 55 × 47 × 40 Å^3. In the presence of high MBP content, the interlamellar space compacts to ∼35 Å. This can only sustain the smallest MBP dimension within the water layer, which is flexible enough to compact down to ∼20 Å, a size corresponding to that of the β-sheet backbone.[13] Recently, a 2D MBP network was proposed to consist of MBP antiparallel dimers, facilitated by weak lateral MBP−MBP interactions.[13] Lateral self-assembly of MBP dimers within the membrane plane would result in a unit cell of approximately 110 and 94 Å. We attribute the two shallow correlation peaks that remain unchanged to in-plane MBP organization within the network. Furthermore, the findings suggest that MBP antiparallel dimers form a weak correlated network in the plane of the membrane that is regulated by the membrane entities (Figure 1C). Therefore, interactions between MBPs and specific lipids are essential for proper MBP network formation.[26] The molecular origins of MBP network destabilization in the presence of modified lipid composition remain unclear; such investigations are beyond the scope of this study.

The compaction of myelin membranes due to the presence of MBP was attributed mainly to electrostatic interactions and counterion release, when entities of opposite charge condense.

DOI: 10.1021/jacs.6b04826
J. Am. Chem. Soc. 2016, 138, 12159−12165

The adhesion between opposing leaflets in the myelin sheath is stabilized by a combination of noncovalent and nonspecific forces, such as van der Waals, hydrophobic, electrostatic forces, and specific short-range interactions mediated by specific amino-acid sequences.[31]

Little is known about the intermolecular interactions and structural organization within myelin sheaths.[32−34] A recent study showed that MBP regulates differently the diffusion rate of specific lipids within the myelin.[26] That indicates specific MBP-lipid interactions that impact the organization and heterogeneity of both the lipids and MBP.

Similar to myelin membrane condensation with MBP, other membrane condensations have been studied before; for example, in the context of nucleic acids with positively charged lipid condensation,[35] or protein−lipid complexes.[36−38] In those instances, condensation due to electrostatic interactions persists up to charge neutrality.[39]

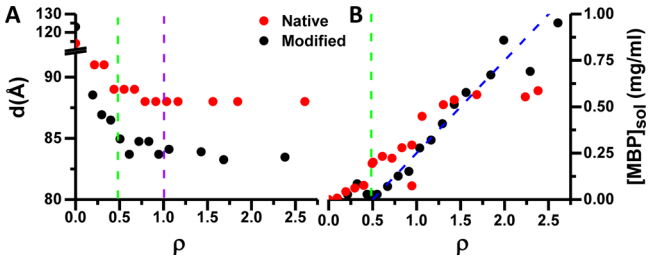

Figure 6. (A) Intermembrane spacing (d) of the dominant lamellar phase as a function of the charge ratio (ρ) between the mole percent of MBP and lipid charges. Compaction proceeds up to $\rho = \rho_c = 1/2$ (green dashed line). The theoretical neutralization limit at $\rho_0 = 1$ is marked with a purple dashed line. (B) Unbound MBP concentration measured above the lipid−protein complex pellet as a function of the charge ratio. For $\rho > \rho_c$, dashed blue line marks linear regression with $[\mathrm{MBP}]_{sol} = 0.5(\rho-\rho_c)$.

Figure 6A shows variations in the lamellar spacing of the dominant correlation peak as a function of the charge ratio, $\rho = Z[\mathrm{MBP}]/[\mathrm{PS}]$. Z represents the net ionized charged groups of MBP, where [MBP] and [PS] represent the mole percent of MBP and phosphatidylserine (PS) under physiological conditions, respectively. For simplicity, we consider PS lipid valence to be one free negative charge, and assume that the valence of MBP (Z) is determined by the total amino acid charge at pH 7.4 (i.e., Z = +21.1). This assumption overestimates Z, as some amino acids may not be exposed to lipids and ions within the intermembrane spacing. Nevertheless, for both lipid compositions, we find that as the charge ratio increases, the lamellar spacing decreases until $\rho = \rho_c = 1/2$ (Figure 6A, green dashed line). Beyond this charge ratio, the lamellar spacing remains constant. These results indicate that condensation persists only up to a fraction of complete charge neutrality (Figure 6A; $\rho_0 = 1$, purple dashed line), and suggest that other intermolecular forces should be taken into account when considering MBP condensation. These include repulsion originating from the minimal dimension of MBP's β-sheet backbone.[13] Similar overcharging phenomena were observed previously in polyelectrolyte-membrane complexes,[36,40] suggesting additional degrees of freedom in the membrane, complexing agent, and surrounding medium.

In most previously studied examples of polyelectrolyte-membrane condensation, the lamellar spacing remained constant during absorption of an additional condensing agent of opposite charge, while the distance between the condensing agents decreases.[35−39] In our case, the dominant lamellar correlation peaks are strongly regulated by addition of MBP, while MBP−MBP correlation peaks remain constant. In both instances, the dominant phase belongs to the lipid intermembrane distance, and the shallow correlation peaks, to the interactions among the various condensing agents (e.g., DNA−DNA or MBP−MBP). We propose that the difference between the two behaviors may be attributed to the interactions between joint MBPs, which form a mesh-like structure (with relatively fixed unit-cell dimensions), while the interbilayer distance decreases, with increasing concentrations of MBPs. Condensation reaches saturation when the water layer is on the order of an MBP thickness layer that cannot be compressed any further.

To estimate MBP encapsulation within the MLV, lipid−protein complexes were centrifuged and the solution containing unbound MBP was separated. In Figure 6B, we show unbound MBP concentrations determined by a Bradford assay as a function of the charge ratio, ρ. As with our SAXS data, we find that below ρ_c (Figure 6B, green dashed line), the concentration of unbound MBP is very low, suggesting full MBP encapsulation within the MLV. Above ρ_c, the unbound MBP concentration increases linearly, with half of the protein remaining in solution, and the other half being encapsulated within the MLV (Figure 6B). This finding demonstrates that membrane compaction saturation is correlated with MBP intake capabilities that change significantly at ρ_c, and suggest that beyond ρ_c additional MBPs extend pre-existing MBP networks.

CONCLUSIONS

We demonstrate that minor alterations in lipid content, as in the diseased case, result with structural instability due to the formation of the H_{II} phase. Furthermore, the transition from the lamellar to the inverted hexagonal phase involves enhanced undulation of the membrane in the vicinity of the H_{II} phase. Such undulations are indeed observed both in vivo and in vitro. Importantly, highly undulated myelin sheaths may lead to local cytosol exposure to the immune system which might initiate the autoimmune response.

We also show that MBP binding to the lipid membrane leads to dramatic rearrangement and morphological changes in the lipid domains. In-plane organization of mesh-like MBP structures is absent in the presence of the modified lipid composition although the proteins still compact the membrane. In such a case, the addition of MBP hinders both local instability and further development of the H_{II} phase.

These results are relevant to MS etiology and targeted diagnostics and demonstrate the critical importance of lipid metabolism and synthesis for the cytoplasmic myelin leaflet. Furthermore, manipulating the lipid composition and MBP content may prevent demyelination and exposure of the cytoplasmic entities to attacks by the immune system.

ASSOCIATED CONTENT

Supporting Information

The Supporting Information is available free of charge on the ACS Publications website at DOI: 10.1021/jacs.6b04826.

Materials and Methods, sample preparation, and analysis (PDF)

DOI: 10.1021/jacs.6b04826
J. Am. Chem. Soc. 2016, 138, 12159−12165

AUTHOR INFORMATION

Corresponding Author

*roy@post.tau.ac.il

Notes

The authors declare no competing financial interest.

ACKNOWLEDGMENTS

We are grateful to Wolfgang Helfrich, Philip Pincus, Cyrus Safinya, Joab Chapman, Jacob Israelachvili, Michael Schick, Cecilia Leal, Michael Kozlov, Avinoam Ben-Shaul, Daniel Harries, and Mikael Simons for useful and enlightening conversations. RS thanks Eti Malka-Gibor and Micha Kornreich for their assistance with measurements. We thank the SAXS beamlines for SAXS measurements: I22 at Diamond Light Source, Oxfordshire, UK; I911-SAXS at MAX IV Laboratory, Lund, Sweden; and P12 EMBL BioSAXS at Hamburg, Germany. The work was supported by the Israel Science Foundation (571/11), the European Community's seventh Framework Programme (CIG - 293402), and the Sackler Institute for Biophysics at Tel Aviv University. Travel grants to synchrotron were provided by BioStruct-X. The cryo-TEM work was performed in the Technion Laboratory for Electron Microscopy of Soft Matter, supported by the Technion Russell Berrie Nanotechnology Institute (RBNI).

REFERENCES

(1) Snaidero, N.; Simons, M. *J. Cell Sci.* **2014**, *127* (Pt 14), 2999.
(2) Chang, K.-J.; Redmond, S. A.; Chan, J. R. *Nat. Neurosci.* **2016**, *19* (2), 190.
(3) Aggarwal, S.; Snaidero, N.; Pähler, G.; Frey, S.; Sánchez, P.; Zweckstetter, M.; Janshoff, A.; Schneider, A.; Weil, M.-T. T.; Schaap, I. a T.; Görlich, D.; Simons, M. *PLoS Biol.* **2013**, *11* (6), e1001577.
(4) Wood, D. D.; Moscarello, M. A. *J. Membr. Biol.* **1984**, *79* (3), 195.
(5) Bakhti, M.; Aggarwal, S.; Simons, M. *Cell. Mol. Life Sci.* **2014**, *71* (7), 1265.
(6) Ozgen, H.; Baron, W.; Hoekstra, D.; Kahya, N. *Cell. Mol. Life Sci.* **2016**, *73*, 3291.
(7) Boggs, J. M. *Cell. Mol. Life Sci.* **2006**, *63* (17), 1945.
(8) Min, Y.; Kristiansen, K.; Boggs, J. M.; Husted, C.; Zasadzinski, J. A.; Israelachvili, J. *Proc. Natl. Acad. Sci. U. S. A.* **2009**, *106* (9), 3154.
(9) Stadler, A. M.; Stingaciu, L.; Radulescu, A.; Holderer, O.; Monkenbusch, M.; Biehl, R.; Richter, D. *J. Am. Chem. Soc.* **2014**, *136* (19), 6987.
(10) Harauz, G.; Boggs, J. M. *J. Neurochem.* **2013**, *125* (3), 334.
(11) Bates, I. R.; Feix, J. B.; Boggs, J. M.; Harauz, G. *J. Biol. Chem.* **2004**, *279* (7), 5757.
(12) Vassall, K. A.; Bamm, V. V.; Harauz, G. *Biochem. J.* **2015**, *472* (1), 17.
(13) Kattnig, D. R.; Bund, T.; Boggs, J. M.; Harauz, G.; Hinderberger, D. *Biochim. Biophys. Acta, Biomembr.* **2012**, *1818* (11), 2636.
(14) Genain, C. P.; Cannella, B.; Hauser, S. L.; Raine, C. S. *Nat. Med.* **1999**, *5* (2), 170.
(15) Ohler, B.; Graf, K.; Bragg, R.; Lemons, T.; Coe, R.; Genain, C.; Israelachvili, J.; Husted, C. *Biochim. Biophys. Acta, Mol. Basis Dis.* **2004**, *1688* (1), 10.
(16) Weissert, R. *J. Neuroimmune Pharmacol.* **2013**, *8* (4), 857.
(17) Sospedra, M.; Martin, R. *Annu. Rev. Immunol.* **2005**, *23*, 683.
(18) Ransohoff, R. M. *Nat. Neurosci.* **2012**, *15* (8), 1074.
(19) Ben-Nun, T.; Ginsburg, A.; Székely, P.; Raviv, U. *J. Appl. Crystallogr.* **2010**, *43* (6), 1522.
(20) Ziblat, R.; Leiserowitz, L.; Addadi, L. *J. Am. Chem. Soc.* **2010**, *132* (28), 9920.
(21) Siegel, D. P.; Green, W. J.; Talmon, Y. *Biophys. J.* **1994**, *66* (2), 402.
(22) Schmitt, S.; Castelvetri, L. C.; Simons, M. *Biochim. Biophys. Acta, Mol. Cell Biol. Lipids* **2015**, *1851* (8), 999.
(23) Koltover, I.; Salditt, T.; Rädler, J. O.; Safinya, C. R. *Science* **1998**, *281* (5373), 78.
(24) Israelachvili, J. N. *Intermolecular and Surface Forces*, 3rd ed.; Elsevier Inc.: Santa Barbara, CA, 2011.
(25) Fuller, N.; Rand, R. P. *Biophys. J.* **2001**, *81* (1), 243.
(26) Steshenko, O.; Andrade, D. M.; Honigmann, A.; Mueller, V.; Schneider, F.; Sezgin, E.; Hell, S. W.; Simons, M.; Eggeling, C. *Biophys. J.* **2016**, *110* (11), 2441.
(27) Lee, D. W.; Min, Y.; Dhar, P.; Ramachandran, A.; Israelachvili, J. N.; Zasadzinski, J. A. *Proc. Natl. Acad. Sci. U. S. A.* **2011**, *108* (23), 9425.
(28) Min, Y.; Alig, T. F.; Lee, D. W.; Boggs, J. M.; Israelachvili, J. N.; Zasadzinski, J. A. *Biophys. J.* **2011**, *100* (6), 1490.
(29) Busch, D. J.; Houser, J. R.; Hayden, C. C.; Sherman, M. B.; Lafer, E. M.; Stachowiak, J. C. *Nat. Commun.* **2015**, *6*, 7875.
(30) Haas, H.; Oliveira, C. L. P.; Torriani, I. L.; Polverini, E.; Fasano, A.; Carlone, G.; Cavatorta, P.; Riccio, P. *Biophys. J.* **2004**, *86* (1), 455.
(31) Hu, Y.; Doudevski, I.; Wood, D.; Moscarello, M.; Husted, C.; Genain, C.; Zasadzinski, J. A.; Israelachvili, J. *Proc. Natl. Acad. Sci. U. S. A.* **2004**, *101* (37), 13466.
(32) Golds, E. E.; Braun, P. E. *J. Biol. Chem.* **1978**, *253* (22), 8162.
(33) Harris, R.; Findlay, J. B. C. *Biochim. Biophys. Acta, Biomembr.* **1983**, *732* (1), 75.
(34) Smith, R. *J. Neurochem.* **1992**, *59* (5), 1589.
(35) Shirazi, R. S.; Ewert, K. K.; Silva, B. F. B.; Leal, C.; Li, Y.; Safinya, C. R. *Langmuir* **2012**, *28* (28), 10495.
(36) Moshe, L.; Saper, G.; Szekely, O.; Linde, Y.; Gilon, C.; Harries, D.; Raviv, U. *Soft Matter* **2013**, *9* (29), 7117.
(37) Yang, L.; Liang, H.; Angelini, T. E.; Butler, J.; Coridan, R.; Tang, J. X.; Wong, G. C. L. *Nat. Mater.* **2004**, *3* (9), 615.
(38) Wong, G. C.; Tang, J. X.; Lin, A.; Li, Y.; Janmey, P. A.; Safinya, C. R. *Science* **2000**, *288*, 2035.
(39) Wagner, K.; Harries, D.; May, S.; Kahl, V.; Rädler, J. O.; Ben-Shaul, A. *Langmuir* **2000**, *16* (2), 303.
(40) Koltover, I.; Salditt, T.; Safinya, C. R. *Biophys. J.* **1999**, *77* (2), 915.

DOI: 10.1021/jacs.6b04826
J. Am. Chem. Soc. 2016, 138, 12159−12165